Highpressure range of the addition of HO to HO. III. Saturated laserinduced fluorescence measurements between 200 and 700 K

D. Fulle, H. F. Hamann, H. Hippler, and J. Troe

Citation: The Journal of Chemical Physics **105**, 1001 (1996); doi: 10.1063/1.471944
View online: http://dx.doi.org/10.1063/1.471944
View Table of Contents: http://scitation.aip.org/content/aip/journal/jcp/105/3?ver=pdfcov
Published by the AIP Publishing

High-pressure range of the addition of HO to HO. III. Saturated laser-induced fluorescence measurements between 200 and 700 K

D. Fulle, H. F. Hamann, H. Hippler, and J. Troe
Institut für Physikalische Chemie, Universität Göttingen, Tammannstrasse 6, D-37077 Göttingen, Germany and Institut für Physikalische Chemie und Elektrochemie, Universität Karlsruhe, Kaiserstrasse 12, D-76128 Karlsruhe, Germany

(Received 6 November 1995; accepted 2 April 1996)

The addition of HO to HO was studied by saturated laser induced fluorescence at temperatures between 200 and 700 K and at pressures of the bath gas helium up to 100 bar. In combination with earlier measurements at 298 K, a set of falloff curves is constructed for the given temperature range. The limiting high-pressure rate constant for the reaction $HO+HO(+He)\rightarrow H_2O_2(+He)$ follows as $k_{1,\infty}=(2.6\pm0.8)\times10^{-11}\ (T/300\ \mathrm{K})^{0\pm0.5}\ \mathrm{cm^3\,molecule^{-1}\,s^{-1}}$, practically independent of the temperature between 200 and 400 K. At higher temperatures, $k_{1,\infty}$ decreases. These results serve as a reference for statistical adiabatic channel model calculations of the recombination rate. © *1996 American Institute of Physics.* [S0021-9606(96)01026-4]

I. INTRODUCTION

The recombination of HO radicals forming H_2O_2

$$HO+HO(+M)\rightarrow H_2O_2(+M), \tag{1}$$

which competes with the bimolecular reaction

$$HO+HO\rightarrow H_2O+O, \tag{2}$$

is of considerable practical importance in atmospheric and combustion chemistry. At the same time, it is of great theoretical interest, because it corresponds to the association of two open-shell radicals on a potential energy surface which is governed by a complicated interplay of long-range dipole–dipole and short-range valence forces.

Summaries of earlier experimental studies of reaction (1), the reverse thermal decomposition of H_2O_2,

$$H_2O_2(+M)\rightarrow HO+HO(+M), \tag{-1}$$

and reaction (2) have been given in Refs. 1–4. The dissociation studies were mostly performed close to the low-pressure limit. Only in some medium pressure shock wave experiments (pressures up to about 40 bar) did some deviations from the limiting low-pressure behavior of reaction (−1) become apparent.[4,5] Recombination experiments[6,7] near room temperature clearly showed deviations from the low-pressure limit; however, because of the difficulties of separating k_1 and k_2, falloff extrapolations toward the high-pressure limit of reaction (1) were unreliable. The situation changed with the recent saturated laser-induced fluorescence (SLIF) study from Ref. 3 (part I of this series) in which a falloff curve of reaction (1) at 298 K was measured up to 140 bar of the bath gas helium. This work allowed for an extrapolation to the high-pressure limit, giving

$$k_{1,\infty}=(2.2\pm0.4)\times10^{-11}\ \mathrm{cm^3\,molecule^{-1}\,s^{-1}} \tag{3}$$

at 298 K. In view of the ongoing discussion about the temperature coefficients of limiting high-pressure rate constants for recombination reactions, it appeared desirable to extend our high-pressure recombination measurements on reaction (1) over as wide a temperature range as possible. This was the aim of the present work. We used for this purpose the SLIF technique described in part I,[3] together with the reaction cells described in part II,[8] in which we studied the reaction $HO+CO\rightarrow H+CO_2$ from 90 to 900 K over the pressure range 1–800 bar. As the experiments for the second-order process HO+HO were more difficult to perform than measurements on the other pseudofirst-order processes studied in parts I and II, only a smaller variation of conditions was possible in the present work. However, in combination with the results from part I, a set of falloff curves could be constructed between 200 and 700 K which allowed for a more systematic study of the properties of $k_{1,\infty}$.

The experimental results about $k_{1,\infty}$ from this work contain information on the activated complex partition function $Q^{\neq}$ of process (1) which represents a thermal average of the number of open channels $W(E,J)$ of the dissociation/association system $H_2O_2\Leftrightarrow 2HO$ (E: total energy; J: total angular momentum of H_2O_2). In combination with the density of states $\rho(E,J)$, $W(E,J)$ also determines the specific rate constant

$$k(E,J)=W(E,J)/h\rho(E,J) \tag{4}$$

for dissociation of H_2O_2 into 2HO. $k(E,\langle J\rangle)$ has been studied before in a variety of overtone excitation measurements (see, e.g., Refs. 4, 9–11). Obviously, experiments on $k_{1,\infty}$ and on $k(E,J)$ should be interpreted together; however, while $k_{1,\infty}$ is only related to $\langle W(E,J)\rangle$, $k(E,J)$ is characterized by the ratio $W(E,J)/\rho(E,J)$. As long as anharmonicity effects in $\rho(E,J)$ are not well characterized,[12] the analysis of $k(E,J)$ is not unambiguous. $\rho(E,J)$ also enters the limiting low-pressure rate coefficient $k_{1,0}$; however, uncertainties in collisional energy transfer parameters here complicate the situation. For this reason, simultaneous analysis of $k_{1,0}$, $k_{1,\infty}$, and $k(E,\langle J\rangle)$ would allow the separate identification of $W(E,J)$, $\rho(E,J)$, and collision energy transfer efficiencies. The present studies of $k_{1,\infty}$ form an essential basis for this analysis.

The number of open channels $W(E,J)$ directly reflects the properties of the $H_2O_2 \Leftrightarrow 2HO$ potential energy surface and of the dynamics on it. While reaction (2) occurs on a H_2O_2-triplet surface (see the theoretical analysis in Ref. 13), reaction (1) concerns the H_2O_2 singlet ground state. *Ab initio* calculations of this potential energy surface[14,15] indicate complicated properties at large HO–HO distances. During the approach of two HO radicals, at first dipole–dipole forces are dominant, before valence forces form a weakly bonded HOHO intermediate; this species can isomerize over a small potential barrier (below the energy of the separated HO radicals) into a HOOH structure which finally forms the strongly valence-bonded hydrogen peroxide in its singlet electronic ground state. Besides the ground state, there are electronically excited potentials which interact with the ground-state potential in a complicated manner. The questions arise to what extent excited electronic states contribute, whether the intermediate potential ridge between the HOHO and HOOH conformations is of kinetic relevance, whether the long-range or the short-range potential govern the kinetics, etc. Measurements of $k_{1,\infty}$ provide an answer to these questions which motivate the present study. In a previous statistical adiabatic channel model (SACM) treatment of the combination of two HO radicals in their lowest rovibronic energy states, we have accounted rigorously[16] for the coupling of all angular momenta of the open shell HO ($^2\Pi_{3/2}$) dipole radicals in terms of Hund's coupling schemes (for a more approximate treatment see also Ref. 17). The calculations for temperatures up to 50 K led to a much larger rate constant $k_{1,\infty}$ than the measured value for 300 K. This result indicated that, out of the manifold of the 16 lowest rovibronic channels (see Ref. 16 for a precise specification of these states), only the lowest one leads to H_2O_2 formation. In order to close the gap to the temperatures of this SACM treatment, we extended the temperatures of our experiments at least down to 200 K. On the theoretical side, a more approximate SACM treatment (neglecting the coupling of rotations with spin and electronic angular momenta) will be given soon[18] which, in contrast to Ref. 16, uses the complete potential from Refs. 14 and 15 and calculates adiabatic channel potential curves such as described in Refs. 19 and 20. The comparison with the present measurements of $k_{1,\infty}$ then will further elucidate the importance of the finer details of the potential.

II. EXPERIMENTAL TECHNIQUE

Our experimental setup was the same as described in parts I and II (Refs. 3 and 8) such that only a few details are given in the following.

HO radicals were produced in appropriate reaction mixtures by laser flash photolysis using excimer lasers (Lambda Physik, EMG 200) either at 193 nm (ArF, 250 mJ per pulse, 17 ns pulse length) or at 248 nm (KrF, 400 mJ, 20 ns). After given time delays, the HO radicals then were detected by laser-induced fluorescence using the pulses from a frequency-doubled (BBO T, 3 mJ, 14 ns) dye laser (Lambda Physik FL 3002). In these experiments either one line of the (0,0) band of HO near 308 nm (Sulforhodamin B) or one line of the (0,1) band near 282 nm (Coumarin 153) was excited. Further details of the optical and electronic arrangement are described in Refs. 3 and 8. The two high-pressure cells used for higher and for lower temperatures have been described in Ref. 8. The preparation of the reaction mixtures, gas handling, and purity of the used substances also have all been characterized in Ref. 8.

III. EXPERIMENTAL RESULTS

Reaction (1) was studied starting from two different reaction mixtures.

At high temperatures mixtures were used which contained 5–10 mbar of N_2O, 20 mbar of H_2O, and high pressures of the bath gas helium. In this case, N_2O was photolyzed at 193 nm [quantum yield of unity, absorption cross section $\sigma_{N_2O} = 5.3 \times 10^{-19} \exp(-590\,\mathrm{K}/T)\,\mathrm{cm}^2\,\mathrm{molecule}^{-1}$, see Ref. 8],

$$N_2O + h\nu \rightarrow N_2 + O(^1D). \tag{5}$$

The formed $O(^1D)$ atoms subsequently reacted with H_2O forming HO via

$$O(^1D) + H_2O \rightarrow 2HO, \tag{6}$$

where $k_6 = 2.2 \times 10^{-10}\ \mathrm{cm}^3\,\mathrm{molecule}^{-1}\,\mathrm{s}^{-1}$.[1] In order to calculate the initial concentration of HO, the following side reactions of $O(^1D)$ with N_2O had to be considered:

$$O(^1D) + N_2O \rightarrow 2NO, \tag{7}$$

$$\rightarrow N_2 + O_2, \tag{8}$$

$$\rightarrow O(^3P) + N_2O, \tag{9}$$

where $k_7 = 7.2 \times 10^{-11}$, $k_8 = 4.4 \times 10^{-11}$, and $k_9 = 1.0 \times 10^{-12}$ $\mathrm{cm}^3\,\mathrm{molecule}^{-1}\,\mathrm{s}^{-1}$,[1] as well as alternative reactions of $O(^1D)$ with H_2O,

$$O(^1D) + H_2O \rightarrow O(^3P) + H_2O, \tag{10}$$

$$\rightarrow H_2 + O_2, \tag{11}$$

where $k_{10} = 1.2 \times 10^{-12}$ and $k_{11} = 2.3 \times 10^{-12}$ $\mathrm{cm}^3\,\mathrm{molecule}^{-1}\,\mathrm{s}^{-1}$, all rate constants given for 298 K from Ref. 1. Reactions (7)–(11) reduce the HO yield in comparison to reaction (6), and lead to NO and $O(^3P)$. From the given rate constants, after consumption of $O(^1D)$, one estimates that the reaction mixture, under our experimental conditions, contained [HO]:[NO]:[$O(^3P)$] on average in the ratio 15:2:1. Initial $O(^1D)$ concentrations, for weak absorptions of the laser light such as was always the case, were calculated from

$$[O(^1D)]_0 = \sigma_{N_2O} F [N_2O]_0 \tag{12}$$

where the fluence F of the laser pulse was recorded by energy gauges (Gentec) and carefully calibrated. The correctness of our determination of the initial HO concentration in part I was controlled via HNO_3 formation after adding excess NO_2.

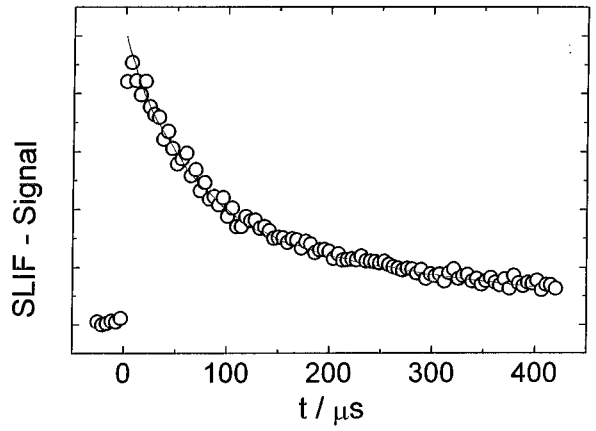

FIG. 1. Saturated laser-induced fluorescence signal of HO disappearance ($T=406$ K; reaction mixture: 9 mbar of N_2O, 20 mbar of H_2O, and 61 bar of He; after photolysis: $[HO]=3.0\times10^{14}$, $[NO]=4.2\times10^{13}$, and $[O(^3P)]=2.1\times10^{13}$ molecule cm^{-3}; solid line: fit with reactions (1), (2), (13), (14), and $k_1=1.8\times10^{-11}$, $k_2=2.3\times10^{-12}$, $k_{13}=2\times10^{-11}$, $k_{14}=3\times10^{-11}$ cm^3 molecule^{-1} s^{-1}).

The decay of HO under our conditions to about 80% was caused by reactions (1) and (2). The remaining about 20% were due to side reactions

$$HO+NO(+M)\rightarrow HONO(+M) \tag{13}$$

and

$$HO+O(^3P)\rightarrow H+O_2, \tag{14}$$

where $k_{13,0}=3.9\times10^{-31}$ $(T/300\ \text{K})^{-2.6}$ [He] cm^6 molecule^{-2} s^{-1}, $k_{13,\infty}=3.3\times10^{-11}$ cm^3 molecule^{-1} s^{-1}, $F_{13,c}(\text{He})\approx1.23\ \exp(-T/815\ \text{K})$ from Refs. 3 and 21, $k_{14}=2.3\times10^{-11}\exp(110\ \text{K}/T)$ cm^3 molecule^{-1} s^{-1}.[1] Further consecutive reactions could be neglected. Our SLIF profiles of HO were fitted, see Fig. 1, to the mechanism of reactions (1), (2), (13), and (14), from which k_1 was derived. The results for k_1+k_2 and the corresponding experimental conditions are given in Table I.

In order to obtain maximum sensitivity of the fit to reactions (1) and (2), the measured points were weighted by a Gaussian distribution centered around the points obtained at 100–150 μs; at shorter times a minor influence of vibrational relaxation of HO had to be accounted for, at later times the contribution from reactions (13) and (14) could not be neglected. Changes of 50% in k_{13} or k_{14} would have resulted in changes of k_1+k_2 by about 6%; the uncertainty in our HO calibration in part I was estimated to lead to an uncertainty of about $\pm30\%$ in k_1 which determines the overall uncertainty of our measurements of k_1+k_2.

TABLE I. Second-order rate coefficients for HO consumption by reactions (1) $HO+HO(+He)\rightarrow H_2O_2(+He)$ and (2) $HO+HO\rightarrow H_2O+O$ ([He] in molecule cm^{-3}, T in K; No. is the number of experiments, k_1+k_2 in cm^3 molecule^{-1} s^{-1}).

[He]	T	No.	k_1+k_2
1.0×10^{21}	210	5	2.5×10^{-11}
8.1×10^{20}	210	5	1.7×10^{-11}
6.4×10^{20}	210	7	1.9×10^{-11}
5.0×10^{20}	210	4	1.8×10^{-11}
3.5×10^{20}	210	5	1.4×10^{-11}
1.6×10^{21}	406	3	1.7×10^{-11}
1.6×10^{21}	510	3	1.3×10^{-11}
1.2×10^{21}	510	3	1.0×10^{-11}
1.0×10^{21}	614	3	8.2×10^{-12}
8.9×10^{20}	694	3	6.0×10^{-12}

At low temperatures mixtures were used which contained less than 1 mbar of O_3, 10–30 mbar of CH_4, and high pressures of the bath gas helium. In this case, photolysis of O_3 at 248 nm,

$$O_3+h\nu\rightarrow O_2+O(^1D) \tag{15}$$

(quantum yield of unity, absorption cross section $\sigma_{O_3}=1.0\times10^{-17}$ cm^2 molecule^{-1})[1] yields $O(^1D)$ atoms which then react with CH_4 to form HO,

$$O(^1D)+CH_4\rightarrow HO+CH_3, \tag{16}$$

where $k_{16}=1.4\times10^{-10}$ cm^3 molecule^{-1} s^{-1}.[1] The side reactions

$$O(^1D)+O_3\rightarrow O(^3P)+O_3, \tag{17}$$

$$\rightarrow 2O_2, \tag{18}$$

$$O(^1D)+CH_4\rightarrow H_2CO+H_2, \tag{19}$$

where $k_{17}=1.2\times10^{-10}$, $k_{18}=1.2\times10^{-10}$, and $k_{19}=1.4\times10^{-11}$ cm^3 molecule^{-1} s^{-1},[1] reduced the HO production by about 10%. Again the absorbed energy from the photolysis laser was measured (Gentec) and from this the generated HO concentration was calculated accounting for the 10% reduction by reactions (17)–(19). In this way, initial concentrations of HO between 8×10^{14} and 3×10^{15} molecule cm^{-3} were obtained. Besides reactions (1) and (2), HO is consumed by reaction (14) and by combination with CH_3,

$$HO+CH_3(+M)\rightarrow CH_3OH(+M), \tag{20}$$

where $k_{20}=6\times10^{-11}$ cm^3 molecule^{-1} s^{-1}.[1] However, the effect of reaction (20) is reduced by the reaction

$$CH_3+CH_3(+M)\rightarrow C_2H_6(+M), \tag{21}$$

where $k_{21}=4\times10^{-11}$ cm^3 molecule^{-1} s^{-1}.[2] Reactions of HO with O_3 [$k=2\times10^{-12}\exp(-1000\ \text{K}/T)$ cm^3 molecule^{-1} s^{-1}][1] and with CH_4 [$k=3.7\times10^{-12}\exp(-1820\ \text{K}/T)$ cm^3 molecule^{-1} s^{-1}][1] could be neglected under our conditions. Fitting of the recorded HO profiles, see Fig. 2, was done with reactions (1), (2), (14), (20), and (21). In the first stage, the profiles are influenced by vibrational relaxation of HO and by reactions (20) and (21); at longer times, reaction (14) becomes more important; between about 20 and 60 μs, the dominance of reactions (1) and (2) is most pronounced such that we weighted these points most strongly again by a Gaussian distribution. The sensitivity of the derived k_1+k_2 was 6%, 10%, 30%, and 30% for changes by 50% of the values of k_2, k_{14}, k_{20}, and k_{21}, respectively. We again estimate the overall uncertainty of k_1+k_2 to be about $\pm30\%$. The derived values of k_1+k_2 are included in Table I.

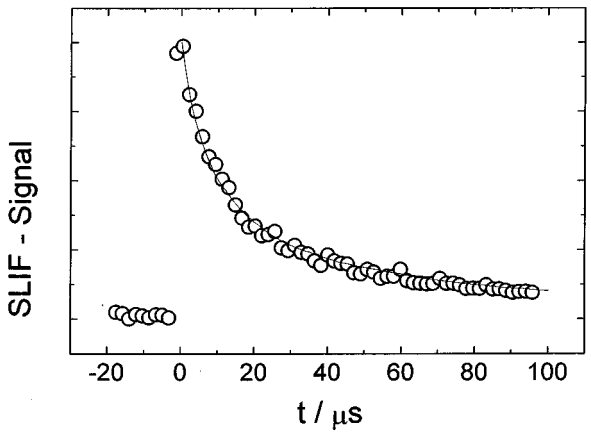

FIG. 2. Saturated laser-induced fluorescence signal of HO disappearance ($T=210$ K; reaction mixture: 38 mbar of CH_4, less than 1 mbar of O_3, and 19 bar of He; after photolysis: $[HO]=[CH_4]=9.2\times10^{14}$ molecule cm^{-3}; solid line: fit with reactions (1), (2), (14), (20), (21), and $k_1=1.8\times10^{-11}$, $k_2=1.4\times10^{-12}$, $k_{14}=3.9\times10^{-11}$, $k_{20}=7\times10^{-11}$, $k_{21}=4\times10^{-11}$ cm^3 $molecule^{-1}$ s^{-1}).

IV. FALLOFF CURVES FOR REACTION (1)

In the following we try to construct a set of falloff curves for reaction (1) with the goal to obtain information on the temperature coefficient of the limiting high-pressure rate constant $k_{1,\infty}$. In the present case this procedure remains somewhat uncertain because of the following reasons:

(i) With increasing temperature there is increasing falloff below the high-pressure limit such that the available experiments increasingly fall below the limit;
(ii) the separation of k_1 and k_2 is not unambiguous and becomes increasingly difficult with increasing temperatures;
(iii) the temperature dependence of $k_{1,0}$, which determines the position of the falloff curve, is not well known experimentally.

Nevertheless, reliable results on $k_{1,\infty}$ appear at least obtainable between 200 and 400 K.

The experimental rate coefficients from Table I correspond to the sum of k_1 and k_2, see the discussion in part I,[3] such that k_2 has to be subtracted. Unfortunately the determination of k_2 still provides a problem. A variety of studies[1,2] has led to values of k_2 in the range $(1.4–2.3)\times10^{-12}$ cm^3 $molecule^{-1}$ s^{-1} at 298 K, with an average value of 1.9×10^{-12} cm^3 $molecule^{-1}$ s^{-1}. Measurements from Ref. 22 led to $k_2=1.4\times10^{-12}$ cm^3 $molecule^{-1}$ s^{-1} at 298 K and a temperature dependence given by $k_2=3.2\times10^{-12}\exp(-242\ \mathrm{K}/T)$ cm^3 $molecule^{-1}$ s^{-1} between 253 and 578 K. However, the scatter of the data prevented an unambiguous separation of k_1 and k_2. Theoretical simulations of k_2 from Ref. 13, when fitted to $k_2(298\ \mathrm{K})=1.9\times10^{-12}$ cm^3 $molecule^{-1}$ s^{-1}, lead to $k_2=2.63\times10^{-20}\ T^{2.62}\exp(+945\ \mathrm{K}/T)$ cm^3 $molecule^{-1}$ s^{-1}. Independent of which determination one prefers, k_2 can amount up to about one-half of the rate constant given in Table I for 694 K and to one-tenth of the rate constants for 210 and 406 K. Therefore, our low-temperature data are much less influenced by the uncertainty in k_2 than our high-temperature data.

The extrapolation of k_1 to $k_{1,\infty}$ strongly depends on the position of the falloff curve along the pressure axis and, hence, on the limiting low-pressure rate constants $k_{1,0}$. Because of the problem of separating k_1 and k_2, these are not known experimentally with sufficient precision. Only at 298 K do the data allow one to check the internal consistency of several measurements, such as the low-pressure data from Refs. 6 and 7 measured in N_2 and the high-pressure data from part I measured in He. Considering the relative bath gas efficiencies $k_{1,0}$ (M=He)/$k_{1,0}$ (M=N_2)$=0.55\pm0.05$ from H_2O_2 thermal dissociation studies,[23] the data were shown to be consistent,[3] although considerable discrepancies between the data from Refs. 6 and 7 await for an explanation. In this situation, it appears more reasonable to base the determination of $k_{1,0}(T)$ on the experimental value of $k_{1,0}$ (298 K, M=He)$=3.7\times10^{-31}$ [He] cm^6 $molecule^{-2}$ s^{-1} from the falloff curve of Ref. 3 and a theoretical simulation of the temperature dependence such as given in Ref. 24. On the basis of this calculation, we represent $k_{1,0}$ by $k_{1,0}=3.7\times10^{-31}$ [He] $(T/300\ \mathrm{K})^{-2.7}$ cm^6 $molecule^{-2}$ s^{-1} for $T\geqslant300$ K and a turnover to a much weaker temperature dependence at $T\leqslant300$ K with $k_{1,0}$ (200 K)$=4.9\times10^{-31}$ [He] and $k_{1,0}$ (250 K)$=4.5\times10^{-31}$ [He] cm^6 $molecule^{-2}$ s^{-1}.

As this is common practice, we represent the falloff curves in reduced form by[25]

$$\frac{k}{k_\infty}=\left(\frac{k_0/k_\infty}{1+k_0/k_\infty}\right)F_c^{\{1+[\log(k_0/k_\infty)/N]^2\}^{-1}}, \tag{22}$$

with $N=0.75-1.27\log F_c$. The theoretical modelling in Ref. 4, although still simplified, indicated that F_c in this case is fairly independent of the temperature, being close to $F_c\approx0.5\pm0.05$ between 200 and 700 K and appropriate for M=He, Ar, and N_2. Uncertainties at this point are minor compared to those of $k_{1,0}$ and the other problems discussed above.

Falloff curves from Eq. (22), using the described values of $k_{1,0}$ and k_2, were compared with the data from Table I and the 298 K data from Ref. 3, leaving $k_{1,\infty}$ as an adjustable parameter.

Figure 3 shows the resulting set of falloff curves, for the temperatures 210, 298, 406, 510, 614, and 694 K (from top to bottom), which were constructed with $k_{1,\infty}=2.6\times10^{-11}$, 2.6×10^{-11}, 2.6×10^{-11}, 1.8×10^{-11}, 1.2×10^{-11}, and 0.65×10^{-11} cm^3 $molecule^{-1}$ s^{-1}, respectively. Because of the less problematic separation of k_1 and k_2 and the smaller extent of falloff below $k_{1,\infty}$, the data for 210–406 K of

$$k_{1,\infty}=(2.6\pm0.8)\times10^{-11}\ \ cm^3\ molecule^{-1}\ s^{-1} \tag{23}$$

are the most reliable. A comparison of the present recombination data with H_2O_2 dissociation results appears useful for several reasons: One may check the reliability of the calculation of $k_{1,0}$ for high temperatures; one may estimate falloff effects in H_2O_2 dissociation studies; and one may control the internal consistency of dissociation and recombination rates and their relation by the equilibrium constant. We do this analysis for 700 K and the bath gas He. Flow and static

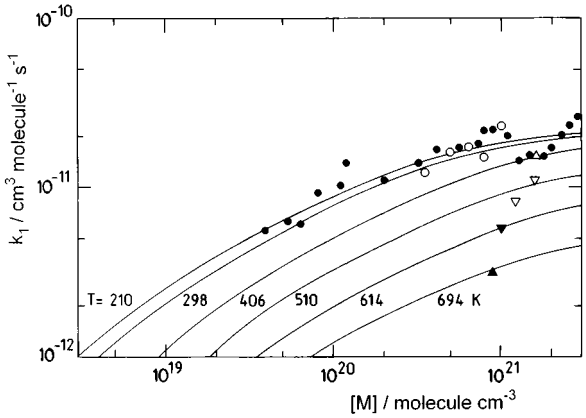

FIG. 3. Falloff curves for the reaction (1) HO+HO (+He)→H_2O_2(+He). Measurements of k_1 at T=210 (○), 298 [●, from part I (Ref. 3)], 406 (△), 510 (▽), 614 (▼), and 694 K (▲) from this work (see Table I with k_2 subtracted); solid lines: falloff curves from Eq. (22) with $k_{1,0}$, $k_{1,\infty}$, and F_c such as given in Sec. IV.

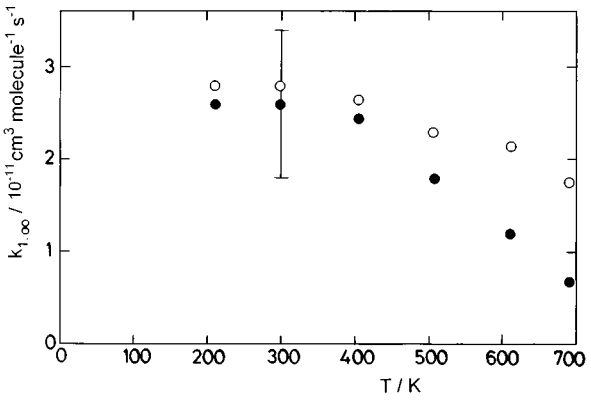

FIG. 4. Limiting high-pressure rate constants $k_{1,\infty}$ for the reaction (1) HO+HO (+M)→H_2O_2(+M) [●: falloff extrapolation of Fig. 3 with k_2 subtraction from k_1+k_2, from Sec. IV; ○: falloff extrapolation of k_1+k_2 neglecting k_2].

system studies in N_2 from several laboratories between 710 and 830 K led to k_{-1}=[N_2] $1.7\times10^{17}\exp(-46\,300$ cal mol^{-1}/RT) cm^3 mol^{-1} s^{-1},[23] which, with a relative rate constant k_{-1} (He) $k_{1,0}/k_{-1}$ (N_2)=0.55±0.02,[23] gives $k_{1,0}$ (700 K)=2.9×10^{-32} [He] cm^6 molecule^{-2} s^{-1} when K_c =1.89×10^{10} molecule cm^{-3} is used.[2] As the flow system studies were made near 1 bar (at 700 K corresponding to 1.05×10^{19} molecule cm^{-3}), the resulting second-order rate constant would have been k_1 (700 K) [He]=3.0×10^{-13} cm^3 molecule^{-1} s^{-1}. Our falloff calculation for these calculations gives $k_{1,0}$ (700 K) [He]=2.7×10^{-13} cm^3 molecule^{-1} s^{-1} in very good agreement, confirming the internal consistency of the treatment at the low pressure end of the falloff curve. However, our falloff calculation also indicates that, for 700 K and 1 bar of He, the measured rate coefficient is only $0.69\times k_{1,0}$ [He], i.e., the rate constants are 30% below the low-pressure limit. Obviously this effect was not identified in the analysis of the H_2O_2 dissociation experiments although it was visible as an intercept in the k_1-P plots of Ref. 23.

The foregoing comparison of recombination and dissociation results confirms the validity of the present construction of falloff curves at the low-pressure end. The high-pressure end exclusively relies on the present measurements. While our measurements at 200–400 K are hardly affected by the uncertainty of k_2 such that $k_{1,\infty}$ from Eq. (23) is well confirmed, the apparent strong decrease of $k_{1,\infty}$ at higher temperatures depends on k_2. If, in the extreme case, k_2 could be completely neglected, our measurement of k_1 at 694 K would lead to $k_{1,\infty}\approx1.8\times10^{-11}$ cm^3 molecule^{-1} s^{-1}. Compared to Eq. (23) this still would indicate a decrease of $k_{1,\infty}$ at temperatures above 400 K. However, the decrease would not much exceed the contribution from the factor $f_{\rm el}=[Q_{\rm el}({\rm HO})]^{-2}$ in the recombination rate constant (where $Q_{\rm el}$ denotes the electronic partition function of HO with $f_{\rm el}$=0.134 for 200 K and $f_{\rm el}$=0.0816 for 700 K). Figure 4 compares the fitted $k_{1,\infty}(T)$ with and without accounting for a contribution of k_2 to the observed HO decays, assuming k_2 to be given by the above-mentioned expressions. More information beyond the limited experimental conclusions is expected from a theoretical analysis of $k_{1,\infty}$.[18]

ACKNOWLEDGMENT

Financial support of this work by the Deutsche Forschungsgemeinschaft (SFB 357 ''Molekulare Mechanismen unimolekularer Prozesse'') is gratefully acknowledged.

[1] R. Atkinson, D. L. Baulch, R. A. Cox, R. F. Hampson, J. A. Kerr, and J. Troe, J. Phys. Chem. Ref. Data **21**, 1125 (1992); (to be published).
[2] D. L. Baulch, C. J. Cobos, R. A. Cox, C. Esser, P. Frank, Th. Just, J. A. Kerr, M. J. Pilling, J. Troe, R. W. Walker, and J. Warnatz, J. Phys. Chem. Ref. Data **21**, 411 (1992).
[3] R. Forster, M. Frost, D. Fulle, H. F. Hamann, H. Hippler, A. Schlepegrell, and J. Troe, J. Chem. Phys. **103**, 2949 (1995) (part I of this series).
[4] L. Brouwer, C. J. Cobos, J. Troe, H.-R. Dübal, and F. F. Crim, J. Chem. Phys. **86**, 6171 (1987).
[5] E. Meyer, H. A. Olschewski, J. Troe, and H. Gg. Wagner, in *12th Symposium (International) on Combustion* (The Combustion Institute, Pittsburgh, 1969), p. 345; J. Troe, Ber. Bunsenges. Phys. Chem. **73**, 946 (1969); H. Kijewski and J. Troe, Helv. Chim. Acta **55**, 205 (1972).
[6] D. W. Trainor and C. W. von Rosenberg, J. Chem. Phys. **61**, 1010 (1974).
[7] R. Zellner, F. Ewig, R. Paschke, and G. Wagner, J. Phys. Chem. **92**, 4184 (1988).
[8] D. Fulle, H. F. Hamann, H. Hippler, and J. Troe, J. Chem. Phys. **105**, 983 (1996), preceding paper (part II of this series).
[9] N. F. Scherer, F. E. Doany, A. H. Zewail, and J. W. Perry, J. Chem. Phys. **84**, 1932 (1986).
[10] X. Luo and T. R. Rizzo, J. Chem. Phys. **96**, 5129 (1992).
[11] L. J. Butler, T. M. Ticich, M. D. Likar, and F. F. Crim, J. Chem. Phys. **85**, 2331 (1986).
[12] J. Troe, Chem. Phys. **190**, 381 (1995).
[13] L. B. Harding and A. F. Wagner, in *22nd Symposium (International) on Combustion* (The Combustion Institute, Pittsburgh, 1988), p. 983.
[14] L. B. Harding, J. Phys. Chem. **93**, 8004 (1989).
[15] L. B. Harding, J. Phys. Chem. **95**, 8653 (1991).
[16] A. I. Maergoiz, E. E. Nikitin, and J. Troe, J. Chem. Phys. **103**, 2083 (1995).
[17] A. G. Wickham and D. C. Clary, J. Chem. Phys. **98**, 420 (1993).
[18] L. B. Harding and J. Troe (unpublished).

[19] A. I. Maergoiz, E. E. Nikitin, and J. Troe, J. Chem. Phys. **95**, 5117 (1991).
[20] A. I. Maergoiz, E. E. Nikitin, and J. Troe, Z. Phys. Chem. **172**, 129 (1991).
[21] D. Fulle, H. F. Hamann, H. Hippler, and J. Troe (unpublished).
[22] G. Wagner and R. Zellner, Ber. Bunsenges. Phys. Chem. **85**, 1122 (1981).
[23] R. R. Baldwin and D. Brattan, in *8th Symposium (International) on Combustion* (The Combustion Institute, Pittsburgh, 1960), p. 110.
[24] J. Troe, J. Chem. Phys. **66**, 4758 (1977); J. Phys. Chem. **83**, 114 (1979).
[25] J. Troe, Ber. Bunsenges. Phys. Chem. **87**, 161 (1983); R. G. Gilbert, K. Luther, and J. Troe, *ibid*. **87**, 169 (1983).